JOURNAL OF MATERIALS SCIENCE 12 (1977) 2081–2086

X-ray topographic studies of cadmium selenide

N. TAJABOR*, D. R. LOVETT
Physics Department, University of Essex, Colchester, UK

The perfection of single crystal platelets of cadmium selenide, as grown from the vapour phase, has been investigated by X-ray projection topography. Individual dislocations, stacking faults, fringe patterns, curvature of the lattice planes, and the effects of precipitates, have been detected. Dislocations have been identified having Burgers vectors $\frac{1}{3}\langle 1\,1\,\bar{2}\,0\rangle$ and $\langle 0\,0\,0\,1\rangle$ with screw, edge, mixed and 60° configurations.

1. Introduction

Investigation of structural defects in CdSe single crystals using X-ray topographic techniques has been carried out previously by Skorakhod and Datsenko [1], who studied under the anomalous transmission mode CdSe platelets grown by sublimation from the vapour having $(1\,1\,\bar{2}\,0)$ surfaces. They observed dislocation loops lying in the basal plane and dislocation lines along the c axis. No indication was given, however, of the Burgers vectors for the dislocations. In addition rosette-shaped defect images were detected and the authors concluded that these are the images of disk-shaped impurity inclusions lying in the basal plane.

In the present study, dislocation axes and Burgers vectors have been determined in cadmium selenide single crystals grown from the vapour. Also, the arrangement of stacking faults, formed during the growth process parallel to the basal plane, and curvature of lattice planes have been investigated.

2. Experimental

To grow the CdSe crystals, a method was used similar to that of Reed and LaFleur [2] to grow ZnTe and modified by Corsini–Mena *et al.* [3] for growing CdS, CdSe and CdTe. 20 g charges of sublimed-grade cadmium selenide were packed between quartz wool plugs and kept at 1050° C. A third plug was placed at a position corresponding to 600° C to form the crystallization zone. The maximum temperature in the furnace (1090° C) occurred between this third plug and the preceeding plug. In this arrangement, when a carrier gas is passed through the charge, with a moderate flow rate, it becomes saturated with the vapour and then desaturation occurs when it passes through the region of maximum temperature. This reduces the possibility of constitutional supercooling in the growth of the crystals at the beginning of the condensation zone. Argon gas with a flow rate of 150 ml min^{-1} was passed through the tube (nitrogen was used alternatively as the carrier gas) and deposition was found to start from a point corresponding to 1025° C. A growth period of 10 h was chosen and crystals formed on the inner wall of the tube at random angles to the flow direction.

The lattice structure of cadmium arsenide crystals grown from the synthesised elements is hexagonal of the wurtzite type with $a = 4.31$ Å and $c = 7.02$ Å. The space group is $C_{6v}^4 - P6_3mc$ (6 mm) and there are two CdSe molecules per unit cell [4]. The crystal habit of cadmium selenide depends on the type of carrier gas. With argon gas, crystals grew with three different habits: (i) needles up to 2.2 cm long having different diameters and growing from one side of the tube and extending to the opposite side, (ii) hexagonal prisms with dimensions approximately 2 cm × 0.2 cm × 0.2 cm and (iii) smooth platelets, the largest with dimen-

*Present address: Physics Department, Ferdowsi University, Mashhad, Iran.

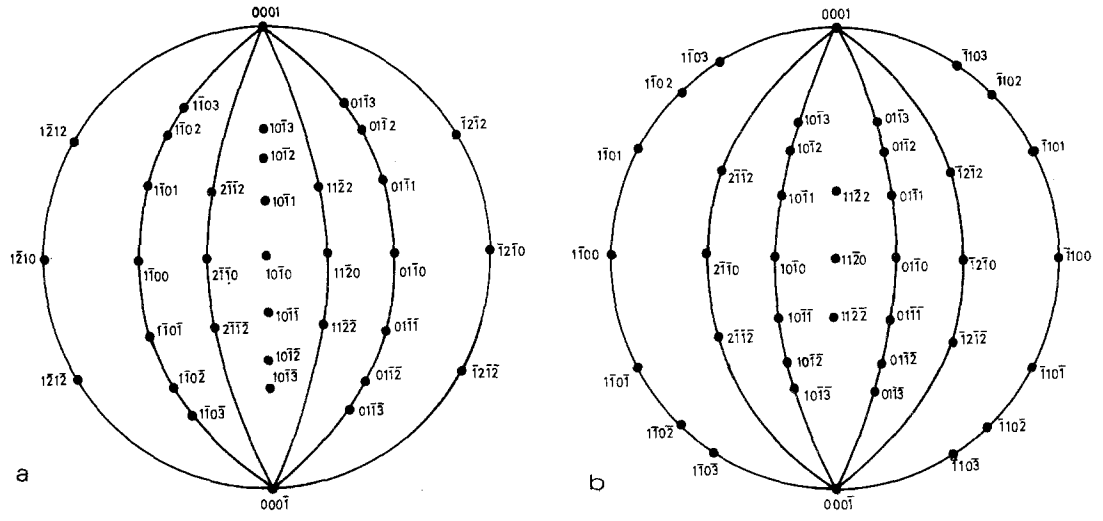

Figure 1 Stereographic projections of some of the planes in CdSe on to (a) (1 0 $\bar{1}$ 0), and (b) (1 1 $\bar{2}$ 0).

sions of 10 mm x 6 mm x 0.02 mm. Laue Photographs of the platelets showed that the major faces of the crystals were of {1 0 $\bar{1}$ 0} or {1 1 $\bar{2}$ 0} types. The *c* axis was usually normal to the longer edges of the platelets. The (1 0 $\bar{1}$ 0) or (1 1 $\bar{2}$ 0) surfaces (but not the ($\bar{1}$ 0 1 0) or ($\bar{1}$ $\bar{1}$ 2 0) faces) showed a number of line-shaped thickness variations aligned parallel or perpendicular to the *c* axis.

Thin as-grown platelets were used for the topographic studies such that no mechanical or chemical polishing was necessary. Cadmium selenide has a relatively high absorption coefficient for X-rays and the $\mu t = 1$ condition, where μ is the absorption coefficient and t the thickness, corresponds to 10 μm for Cu$K\alpha$ radiation, 37 μm for Mo$K\alpha$ and 70 μm for Ag$K\alpha$. Topographs were obtained using a Lang camera and a standard Philips generator, type PW1130, with fine focus air-insulated tubes with silver, molybdenum or copper targets. A tube-to-sample distance of 1.35 m was used. Recording of the topographs was on Ilford L4 nuclear emulsions of 50 μm thickness and topographs are reproduced here as positives. Samples were chosen of approximately 50 μm thickness and included platelets with main surfaces of (1 0 $\bar{1}$ 0) type and others with main surfaces of (1 1 $\bar{2}$ 0) type. Fig. 1 gives stereographic projections of the main planes on to the (1 0 $\bar{1}$ 0) and (1 1 $\bar{2}$ 0) planes.

3. Results and discussion

3.1. The {1 0 $\bar{1}$ 0} samples

Fig. 2 shows a typical topograph obtained from sample a using Ag$K\alpha$ ($\mu t \simeq 0.7$) and the $\bar{1}$ 2 $\bar{1}$ 0 reflection (i.e. from the prismatic plane perpendicular to the crystal face). This was one of a number of reflections for which topographs were obtained. The bottom of the crystal was not of uniform thickness and this caused variation of the reflected intensity. Strain had earlier been put into the specimen at the bottom right-hand corner during a thickness measurement. The dark spots scattered over the topograph are the images of dislocations perpendicular or inclined to the crystal surface with Burgers vectors along the *c* axis. The arrow-shaped area outlined in the central part of the topograph is produced by a "rib" which is terminated on a series of ridges on the surface, and which could be observed optically on a light micrograph. Two parallel dislocation lines, extending from the top edge to a (horizontal) striation

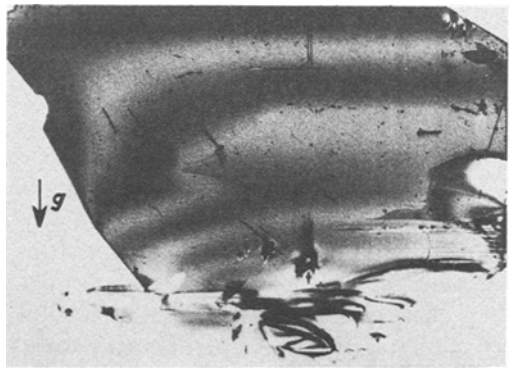

Figure 2 X-ray topograph of sample a ({1 0 $\bar{1}$ 0} growth habit) using Ag$K\alpha$ radiation and the $\bar{1}$ 2 $\bar{1}$ 0 reflection. (x 14).

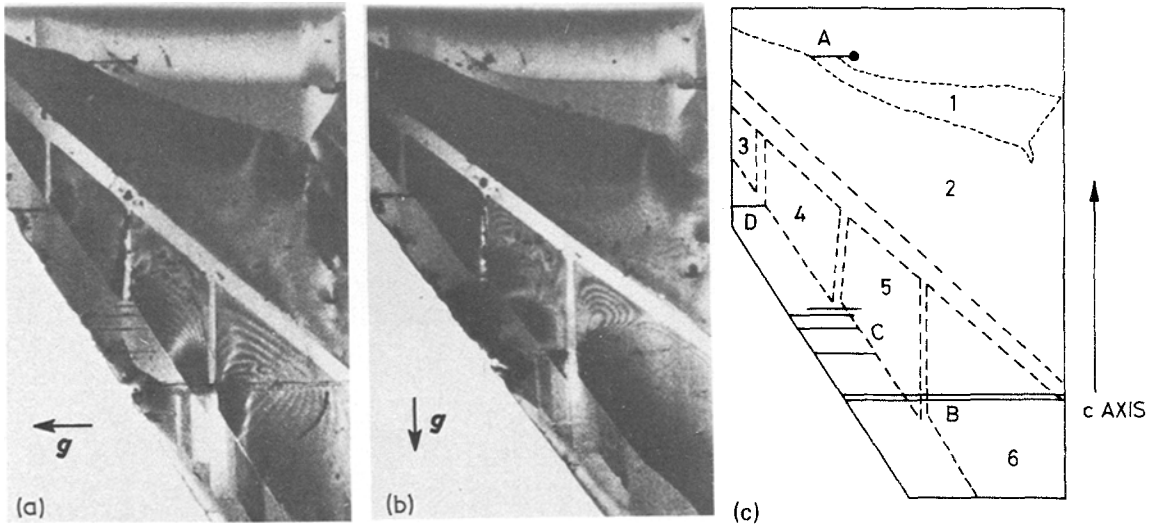

Figure 3 X-ray topographs of sample b ($\{1\,0\,\bar{1}\,0\}$ habit); (a) $1\,\bar{2}\,1\,0$ reflection, (b) $1\,0\,\bar{1}\,\bar{3}$ reflection and (c) key to the main features. (X 30).

line, and further to the right a bundle of dislocations radiating from the dark disk, which may be the image of inclusions of impurity particles, are deduced to be pure screw dislocations with Burgers vectors $\pm\frac{1}{3}[\bar{1}\,2\,\bar{1}\,0]$. The dark line on the right-hand side of the topograph is parallel to the c axis and is not visible in the (0 0 0 2) reflection. It is an image of a pure edge dislocation also with the Burgers vector $\pm\frac{1}{3}[\bar{1}\,2\,\bar{1}\,0]$.

From the projection topographs of other reflections, it was found that there was a higher density of scattered dark spots from the $1\,0\,\bar{1}\,3$ reflection than from the 0 0 0 2 reflection, particularly in the central region of the topograph. It was concluded that these were mainly images of dislocation lines lying in the basal plane and having Burgers vectors parallel to one of the $\langle 1\,1\,\bar{2}\,0\rangle$ directions. Topographs were also obtained using Cu$K\alpha$ radiation under the anomalous transmission condition with $\mu t \simeq 5$. The lower area did not produce contrast, indicating that the crystal was highly deformed here, but elsewhere dislocation lines and growth defects on the surface appeared with light contrast.

Sample b had a main face which had a mirror-like surface, and an opposite face which contained several striations parallel to the c axis. It had a thickness of 60 μm and Ag$K\alpha$ radiation was used to produce projection topographs. Unlike sample a, this sample contained very few dislocations perpendicular to the $(1\,0\,\bar{1}\,0)$ surface, but rather more parallel to the face. Fig. 3 shows two typical topographs for this sample together with a key drawing. Dislocations A, B and C which are visible in Fig. 3a for the $1\,\bar{2}\,1\,0$ reflection were also visible in the $\bar{1}\,1\,0\,0$ and $0\,\bar{1}\,1\,0$ reflections but were invisible in the 0 0 0 2 and $1\,0\,\bar{1}\,\bar{3}$ reflections. It was deduced that these are pure screw dislocations with Burgers vectors $\pm\frac{1}{3}[1\,1\,\bar{2}\,0]$. The D dislocation vanished in the 0 0 0 2 topograph and produced weak contrast in the $\bar{1}\,1\,0\,0$ topograph. Consequently, it is a 60° dislocation lying in the basal plane along the $[1\,\bar{2}\,1\,0]$ direction with the Burgers vector $\pm\frac{1}{3}[1\,1\,\bar{2}\,0]$. As expected for the condition of low absorption topography (i.e. $\mu t < 1$), the dislocation images are darker than the background and the image structure is the same in pairs of topographs taken from opposite sides of a given Bragg plane.

It can be seen from the topographs that the diffracted image of the crystal is divided into distinct regions of low and enhanced intensity. The strips of low intensity are highly perfect parts. The intensity distribution over these areas is more uniform on the original plates than in the reproductions. The thickness of the crystal between regions 1 and 2 changed with a sharp saw-toothed boundary which was not oriented along a definite crystallographic direction. The rest of the crystal was of uniform thickness, except for small variations due to the striations.

Fringes of various shapes appear in the areas numbered 2 to 6. Fringes in regions 2 and 3 were best visible in the $\bar{1}\,1\,0\,0$ and $0\,\bar{1}\,1\,0$ topographs.

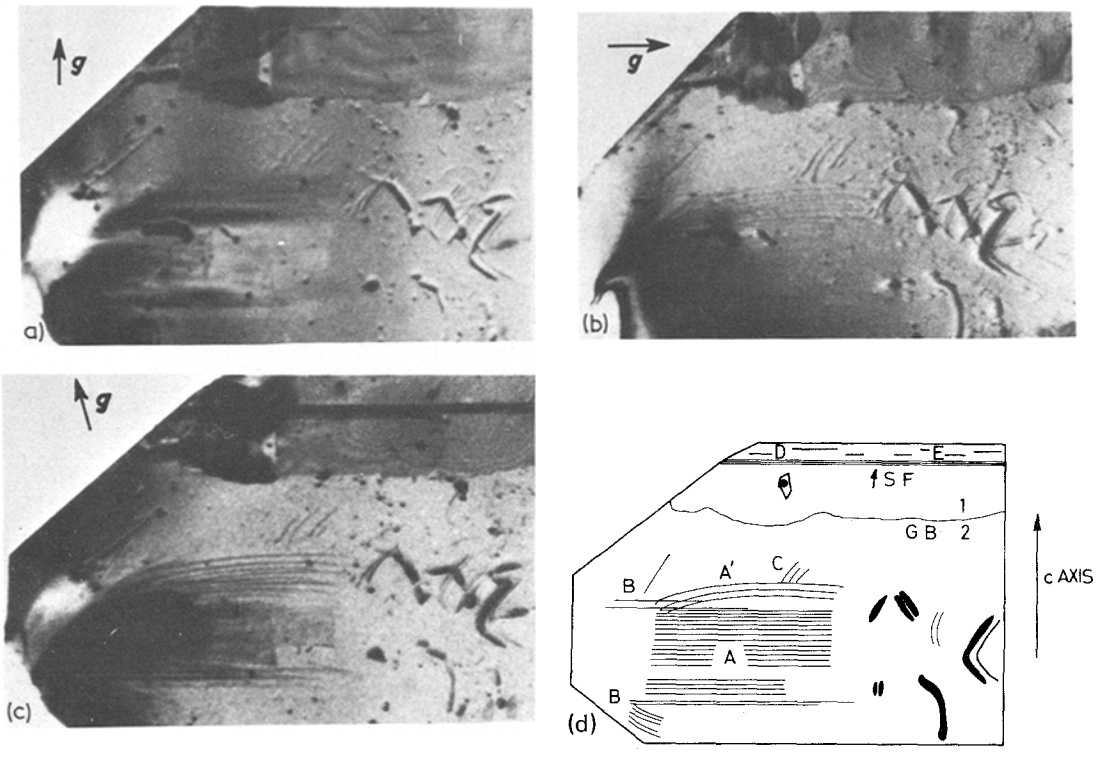

Figure 4 X-ray topographs of sample c ($\{1\,1\,\bar{2}\,0\}$ habit); (a) 0 0 0 2, (b) $\bar{2}$ 1 1 0 and (c) 1 0 $\bar{1}$ 3 reflections and (d) key to the main features. (× 30).

They do not change shape in these topographs, whereas fringes in regions 5 and 6 do. The fringes in 5 and 6 in the 1 $\bar{2}$ 1 0 topograph (Fig. 3a) have an entirely different shape to those in corresponding regions in the other topographs, although the shapes of the fringes are similar for pairs of topographs from a given Bragg plane.

Fringes observed in X-ray topography may be divided into four distinct categories: (i) fringe patterns due to the fault surfaces [5, 6], (ii) Pendellösung fringes [7], (iii) X-ray moiré fringes [8, 9] and (iv) fringe patterns associated with long-range strains [10]. There is no phase difference between rays passing through perfect and faulted layers in reflections for which $h - k = 3n$ (or 0) [11], and therefore the fringes observed here are not due to fault surfaces. They cannot be Pendellösung fringes as their spacings do not change with changes of radiation wavelength, nor between reflections from different Bragg planes. For Moiré fringes, if X-rays pass through successive lattices having reciprocal vectors g_1 and g_2, then the reciprocal of the lattice spacing D of the moiré pattern is given by $g_1 - g_2$, so that $D(nh\,nk\,nl) = (1/n)D(hk\,l)$ for topographs of the $h\,k\,l$ and $nh\,nk\,nl$ reflections. It was found that either the fringes for such pairs did not change their spacing or they disappeared completely in one topograph of the pair. It was deduced, however, that the fringes are compatible with the presence of long-range strain, under which circumstances distorted parts of the crystal should exhibit enhancement in the integrated intensity and the form of the fringe pattern should be the same in topographs from $(h\,k\,l)$ and $(\bar{h}\,\bar{k}\,\bar{l})$ planes. The fringe spacing should decrease with increase of the strain gradient. Strains appear on the topographs confined between boundaries having definite crystallographic directions. It is not clear what mechanism is producing the strains, but striation in the crystal surface may be producing overlapping internal strain fields, and impurity centres may also be giving rise to strain fields. Skorakhad and Datsenko [1] also observed fringe patterns and concluded that there were large segregations of excess Cd and Se at the points in their samples from where the fringes originated.

3.2. The $\{1\,1\,\bar{2}\,0\}$ samples

The sample of this type which was investigated in most detail (sample c) was of thickness 150 μm ($\mu t = 2.1$ for Ag$K\alpha$ radiation). It showed no striations on the main surface but was slightly curved

at the two extremes of its length, which was parallel to the $[1\,\bar{1}\,0\,0]$ direction. A large number of topographs were obtained for different selected Bragg planes, mainly using Ag$K\alpha$, but also Cu$K\alpha$ radiation. Fig. 4 shows topographs from the $(0\,0\,0\,2)$, $(\bar{2}\,1\,1\,0)$ and $(1\,0\,\bar{1}\,3)$ planes, using Ag$K\alpha$ radiation.

It can be seen that dislocations marked as type A mainly vanish for the $0\,0\,0\,2$ reflection (Fig. 4a) and also the $0\,0\,0\,\bar{2}$ reflection, and hence have Burgers vectors along one of the $[1\,1\,\bar{2}\,0]$ directions lying in the basal plane. They have weak contrast in the $\bar{2}\,1\,1\,0$ reflection (Fig. 4b) and also in the $2\,\bar{1}\,\bar{1}\,0$, $1\,\bar{2}\,1\,0$ and $\bar{1}\,2\,\bar{1}\,0$ reflections, and it is deduced that their Burgers vectors are in the $[1\,1\,\bar{2}\,0]$ direction, perpendicular to the crystal surface. The B dislocations can be seen in the $0\,0\,0\,2$, but not in the $\bar{2}\,1\,1\,0$, topographs, conditions which would be met by pure edge dislocations parallel to the $[\bar{2}\,1\,1\,0]$ direction with the Burgers vector along the c axis, i.e. $\boldsymbol{L} = \boldsymbol{g} = [\bar{2}\,1\,1\,0]$, $\boldsymbol{b} = \langle 0\,0\,0\,1\rangle$ and $\boldsymbol{b}\cdot\boldsymbol{g} = 0$ (where $\boldsymbol{L}$ is the dislocation axis and $\boldsymbol{g}$ is a unit vector normal to the Bragg plane).

From the difference in contrast of the dislocations in group A, it can be deduced that they are located at different depths within the crystal. Eight curved dislocations on the side further from the lower edge of the topographs exhibit more contrast and in most of the topographs appear sharper than the others. They are nearer to the X-ray exit surface and are referred to as group A^1. The dislocations reveal themselves by producing direct images with dark contrast in all topographs taken with Ag$K\alpha$ radiation, and by producing Borrmann images with light contrast in those topographs taken with Cu$K\alpha$ radiation. No change of contrast was observed between $h\,k\,i\,l$ and $\bar{h}\,\bar{k}\,\bar{i}\,\bar{l}$ reflections. The contrast behaviour of the group A^1 of dislocations was similar to that of A, except in the pair of topographs taken from the $(1\,0\,\bar{1}\,3)$ and $(\bar{1}\,0\,1\,3)$ Bragg planes; the images of the A^1 dislocations appear with dark contrast in the $1\,0\,\bar{1}\,3$ reflection, and with light contrast in the $\bar{1}\,0\,1\,3$ reflection. This can be seen in Fig. 4c and is a local failure of Friedel's law, which occurs due to the tie-point migration as a result of the curvature of the lattice plane.

Reference to the projection topograph of the $0\,0\,0\,2$ reflection (Fig. 4a) shows broken lines parallel to the top edge; these are separately marked D and E in Fig. 4d and are displaced by a few microns along the c axis; they have a line direction parallel to the $1\,\bar{1}\,0\,0$ direction. They vanish in a pair of $1\,\bar{1}\,0\,0$ Bragg reflections and produce very weak contrast in the projection topographs of $(\bar{2}\,1\,1\,0)$ planes (Fig. 4b and $(1\,\bar{2}\,1\,0)$ planes. Consequently, they are pure edge dislocations having their Burgers vectors parallel to the c axis; $\boldsymbol{b} = \langle 0\,0\,0\,1\rangle$.

In Fig. 4c there are three horizontal dark lines (lettered S.F.) arising from stacking faults (the lines vanish for the $\{1\,1\,\bar{2}\,2\}$ Bragg planes, and also for $(0\,0\,0\,2)$, $(0\,0\,0\,\bar{2})$, $(\bar{2}\,1\,1\,0)$, $(2\,\bar{1}\,\bar{1}\,0)$ and $(\bar{2}\,1\,1\,\bar{2})$). The two types of basal faults with displacement vector $R = \frac{1}{3}[\bar{1}\,1\,0\,0]$ and $R = \frac{1}{6}[\bar{2}\,2\,0\,3]$ respectively, do not produce any contrast for reflections with $h - k = 3n$ (or 0) and $l =$ even. The prismatic fault with $R = \frac{1}{2}[1\,0\,\bar{1}\,1]$ produces contrast, for instance, in the reflection from the $(2\,\bar{1}\,\bar{1}\,0)$ Bragg plane [12]. Therefore, the faults produced here are basal faults. The lowest index reflection which can be used to differentiate between both types of basal fault is the $0\,3\,\bar{3}\,1$ reflection, but it was not possible to get a reflection from the $(0\,3\,\bar{3}\,1)$ plane. This was mainly due to the low reflectivity of the plane (it has an intensity which is less than 1% of the intensity of the $1\,0\,\bar{1}\,0$ reflection), but also, because of the plane's position relative to the crystal surfaces, the diffracted beam would be absorbed out. However, from the successive occurrence of these faults, which run from the top to the bottom of the crystal, it is suggested that they were formed during crystal growth and have fault vector of $\frac{1}{6}[\bar{2}\,2\,0\,3]$. Whenever images of these faults were visible, the images appeared with dark contrast for both topographs taken for each pair of Bragg planes, except in the case of the pair of topographs obtained for the $1\,0\,\bar{1}\,0$ and $\bar{1}\,0\,1\,0$ reflections where the faults produced dark contrast in the $\bar{1}\,0\,1\,0$ reflection and light contrast in the $1\,0\,\bar{1}\,0$ reflection. This implies that the $(1\,0\,\bar{1}\,0)$ lattice planes at the faulted layers are curved with the radius of curvature parallel to the $[\bar{1}\,0\,1\,0]$ direction.

Precipitate particles in the sample have produced a large number of dark spot images on the topographs. Direct images are produced, each with dark contrast and a light shadow which changes its position from one side of the direct image to the other for change of the Bragg plane from $(h\,k\,i\,l)$ to $(\bar{h}\,\bar{k}\,\bar{i}\,\bar{l})$. The direct image is divided into two parts by a contrast-free plane; the direct image of a circular precipitate consists of two dark semicircles

and a single contrast-free plane. On the photographic plates, the contrast-free planes are more clearly observed, but due to the strong contrast of the direct images they are not clear in reproduction. Some of the semicircles and their contrast-free planes can, however, be seen in Fig. 4a. Most of these imperfections are located near to the X-ray entrance surface. (This was established by rotating the crystal through 180° and taking topographs from $(1\,\bar{1}\,0\,0)$ planes; the contrast-free planes of the images were much clearer and the widths of the shadows were reduced).

There is considerable non-uniformity of background intensity over the topographs. Each topograph is divided into distinct regions 1 and 2 by a grain boundary (GB). The intensity over region 1 is stronger than over region 2. The former part exhibits fringe patterns of the type previously discussed. This part showed enhanced intensity on all the pairs of topographs from a given Bragg plane except for the $0\,1\,\bar{1}\,\bar{3}$ reflections; the $0\,\bar{1}\,1\,\bar{3}$ showed strongly increased intensity and the $0\,1\,\bar{1}\,\bar{3}$ exhibited a reduced intensity. The same intensity distribution behaviour was observed around the area where the A dislocations are located, whereas a reversal behaviour was noticed over the region 2 of the topographs. This indicates that due to the long-range strains, the lattice planes are curved with different senses of curvature. Comparison between topographs of the 0002 type reflections and various Bragg planes in the [0001] zone led to the conclusions that the lattice plane curvature has a cylindrical shape with the axis of the cylinder either parallel to the [0001] direction or parallel to the $[1\,1\,\bar{2}\,0]$ direction.

Other platelet samples were investigated of $\{1\,1\,\bar{2}\,0\}$ habit, in particular sample d grown from lower quality starting material (electronic grade). This latter sample gave a higher level of scattered radiation than was observed in other samples because of a high density of impurities, and exhibited a large number of dislocations, with screw, edge, mixed and 60° configurations.

4. Conclusion

Most of the dislocation configurations observed in the samples have been detected previously in other binary compounds with the wurtzite structure (e.g. AlN, CdS, ZnS, ZnSe). Table I summarizes the dislocation axes, Burgers vectors and glide planes involved. Stacking faults have been observed and it is suggested that the Burgers vectors of the partial dislocations are $\frac{1}{6}[\bar{2}\,2\,0\,3]$. Fringes are observed on many of the topographs as a consequence of the presence of internal stress arising from such features as striations and the presence of impurity atoms. Curvature of the lattice planes is also present.

TABLE I Axis directions, Burgers vectors and glide planes of dislocations occurring in cadmium selenide.

Dislocation axis L	Burgers vector b	Angle between L and b	Glide plane
$\langle 1\,\bar{2}\,1\,0\rangle$	$\langle 1\,\bar{2}\,1\,0\rangle/3$	0°	—
$\langle 1\,\bar{2}\,1\,0\rangle$	$\langle \bar{2}\,1\,1\,0\rangle/3$	60°	$\{0\,0\,0\,1\}$
$\langle 1\,\bar{2}\,1\,0\rangle$	$\langle 0\,0\,0\,1\rangle$	90°	$\{1\,0\,\bar{1}\,0\}$
$\langle 0\,0\,0\,1\rangle$	$\langle 1\,\bar{2}\,1\,0\rangle/3$	90°	$\{1\,0\,\bar{1}\,0\}$
$\langle 1\,\bar{1}\,0\,0\rangle$	$\langle 0\,0\,0\,1\rangle$	90°	$\{1\,1\,\bar{2}\,0\}$
$\langle \bar{1}\,1\,0\,1\rangle$	$\langle 0\,0\,0\,1\rangle$	43°	$\{1\,1\,\bar{2}\,0\}$

Acknowledgements

The authors would like to thank Mr E. Adair for the preparation of photographic prints. One of us (N.T.) received financial support from the Iranian Ministry of Science and Higher Education and from the Ferdowsi University (Mashhad, Iran).

References

1. M. YA. SKORAKHOD and L. I. DATSENKO, *Sov. Phys. Cryst.* **13** (1968) 459.
2. T. B. REED and W. J. LAFLEUR, "Solid State Research", Part 1 (MIT, 1968) 20.
3. A. CORSINI-MENA, M. ELLI, C. PAOROCI and L. PELOSINI, *J. Cryst. Growth*, 8 (1971) 297.
4. W. ZACHARIASEN, *Z. Physik Chem.* **124** (1926) 436.
5. A. AUTHIER, D. MILNE and M. SAUVAGE, *Phys. Stat. Sol.* **26** (1968) 469.
6. A. R. LANG, *Z. Naturforsch* **27A** (1972) 461.
7. N. KATO and A. R. Lang, *Acta Cryst.* **12** (1959) 787.
8. J. CHIKAWA, *Appl. Phys. Lett* 7 (1965) 193.
9. A. R. LANG and V. F. MIUSCOV, *ibid* 7 (1965) 214.
10. Y. ANDO and N. KATO, *Acta Cryst.* **21** (1966) 284.
11. H. BLANK, P. DELAVIGNETTE, R. GEVERS and S. AMELINCKX, *Phys. Stat. Sol.* 7 (1964) 747.
12. C. M. DRUM, *Phil. Mag.* **11** (1965) 313.

Received 17 November 1976 and accepted 11 March 1977